

Nuclear receptor binding protein 1 regulates intestinal progenitor cell homeostasis and tumour formation

Catherine H Wilson^{1,7}, Catriona Crombie¹,
Louise van der Weyden¹,
George Poulgiannis², Alistair G Rust¹,
Mercedes Pardo¹, Tannia Gracia^{1,8}, Lu Yu¹,
Jyoti Choudhary¹, Gino B Poulin³,
Rebecca E McIntyre¹, Douglas J Winton⁴,
H Nikki March⁴, Mark J Arends^{5,9},
Andrew G Fraser^{1,6,9} and David J Adams^{1,9,*}

¹Wellcome Trust Sanger Institute, Wellcome Trust Genome Campus, Hinxton, UK, ²Division of Signal Transduction, Beth Israel Deaconess Medical Center and Department of Systems Biology, Harvard Medical School, Boston, MA, USA, ³Faculty of Life Sciences, University of Manchester, Manchester, UK, ⁴Cancer Research UK Cambridge Research Institute, Cambridge, UK, ⁵Department of Pathology, Addenbrookes Hospital, University of Cambridge, Cambridge, UK and ⁶The Donnelly Centre, University of Toronto, Toronto, Canada

Genetic screens in simple model organisms have identified many of the key components of the conserved signal transduction pathways that are oncogenic when misregulated. Here, we identify *H37N21.1* as a gene that regulates vulval induction in *let-60(n1046gf)*, a strain with a gain-of-function mutation in the *Caenorhabditis elegans* Ras orthologue, and show that somatic deletion of *Nrbp1*, the mouse orthologue of this gene, results in an intestinal progenitor cell phenotype that leads to profound changes in the proliferation and differentiation of all intestinal cell lineages. We show that *Nrbp1* interacts with key components of the ubiquitination machinery and that loss of *Nrbp1* in the intestine results in the accumulation of *Sall4*, a key mediator of stem cell fate, and of *Tsc22d2*. We also reveal that somatic loss of *Nrbp1* results in tumourigenesis, with haematological and intestinal tumours predominating, and that nuclear receptor binding protein 1 (*NRBP1*) is downregulated in a range of human tumours, where low expression correlates with a poor prognosis. Thus *NRBP1* is a conserved regulator of cell fate, that plays an important role in tumour suppression.

The EMBO Journal (2012) 31, 2486–2497. doi:10.1038/emboj.2012.91; Published online 17 April 2012

Subject Categories: signal transduction; molecular biology of disease

Keywords: intestine; progenitor cell; Ras; tumour suppressor gene; WNT

*Corresponding author. Experimental Cancer Genetics, Wellcome Trust Sanger Institute, Wellcome Trust Genome Campus, Hinxton, Cambridgeshire CB10 1SA, UK. Tel.: +44 (0)1223 834 244; Fax: +44 (0)1223 496 802; E-mail: da1@sanger.ac.uk

⁷Present address: Department of Biochemistry, Cambridge University, 80 Tennis Court Road, Cambridge CB2 1GA, UK

⁸Present address: Department of Medical Genetics and Division of Renal Medicine, University of Cambridge, Cambridge, UK

⁹Co-senior authors

Received: 18 July 2011; accepted: 6 March 2012; published online 17 April 2012

Introduction

Perturbation of RAS, WNT or NOTCH signalling in the *C. elegans* vulva results in defects in vulval development, and many genetic screens have exploited this fact to identify important components of these pathways. In humans, the RAS, WNT and NOTCH pathways play an important role in orchestrating embryonic development and may be dysregulated in tumourigenesis. In the intestine, these pathways play critical roles in lineage specification and are essential for the normal formation of the bowel. Importantly, stem cells at the base of the intestinal crypt express the leucine-rich repeat-containing G-protein coupled receptor 5 (*Lgr5*) and are the progenitors from which all other cell types of the intestine (enterocytes, Paneth cells, goblet cells and enteroendocrine cells) are generated. Daughter cells of the *Lgr5*⁺ stem cells, called transit-amplifying cells, divide every 12–16 h generating some 300 cells per crypt per day and drive the replenishment of the intestinal epithelium, which is completely renewed every 5 days (Barker *et al*, 2009). Therefore, disruption of the fine balance between differentiation and proliferation by perturbing key signalling pathways has a profound effect on the ability of the intestine to regenerate and function.

Using RNAi in *C. elegans*, we performed a kinome-wide screen and identified the worm orthologue (*H37N21.1*) of the nuclear receptor binding protein 1 (*NRBP1*) as a novel enhancer of the RAS-induced multivulval phenotype (*Muv*) in a *let-60(1046gf)* gain-of-function mutant background. *NRBP1* is located on human chromosome 2p23 and encodes a 535 amino-acid protein. It is ubiquitously expressed and highly conserved (Hooper *et al*, 2000). *NRBP1* is a pseudokinase because it lacks critical catalytic residues in the kinase core, and carries a highly degraded ATP-binding site (Boudeau *et al*, 2006). In addition to its kinase-like domain, *NRBP1* has a putative binding domain for Src homology-2-containing proteins, nuclear export signals, a nuclear localisation signal, a BC-box motif and a binding site for the myeloid leukaemia factor 1 (Gluderer *et al*, 2010). Here, we show that somatic deletion of *Nrbp1* in the mouse causes a progenitor cell phenotype that disrupts the normal programme of cellular differentiation and proliferation along the intestinal crypt–villus axis. We also show that knock-down of *NRBP1* cooperates with *Ras*^{V12} to elicit transformation. Importantly, we show that loss of *Nrbp1* increases the level of *Sall4* and *Tsc22d2* in the intestine where they associate with *Nrbp1* and components of the ubiquitination machinery. In addition, we reveal that *Nrbp1* is a tumour suppressor in mice and that *NRBP1* is downregulated in a range of human cancers where low expression is associated with a poor clinical outcome. Thus, we identify critical roles for an uncharacterised gene through a combination of genetic screening in the worm and detailed functional analysis in the mouse and in human cells.

Results

Identification of H37N21.1 in a kinome-wide RNAi screen in *let-60(n1046gf)* worms

C. elegans that are homozygous for a gain-of-function allele of the worm *Ras* orthologue *let-60(n1046gf)* have a partially penetrant Muv phenotype with ~60% of worms being Muv at 16 °C. The *let-60(n1046gf)* allele encodes an activating mutation in LET-60 that is functionally analogous to the codon 13 Gly > Glu mutation in *RAS* found in human tumours (Beitel *et al*, 1990). Multiple genetic screens have been carried out to identify genes whose loss suppresses the Muv phenotype in *let-60(n1046gf)* animals, and these have resulted in the isolation of many oncogenes acting in the RAS signalling pathway. Here, we use RNAi to identify genes whose loss enhances the Muv phenotype of *let-60(n1046gf)* reasoning that orthologues of these genes might function as tumour suppressors by perturbing the WNT, NOTCH or RAS pathways, which are critical to the formation of the worm vulva. This is the first such screen for enhancers of the Muv phenotype in *let-60(n1046gf)*.

We adapted standard RNAi screening protocols (Fraser *et al*, 2000) to establish screening conditions in which we could robustly identify three previously characterised enhancers (*egr-1*, *egl-27* and *nhl-2*) (Solari and Ahringer, 2000; Hammell *et al*, 2009) of the *let-60(n1046gf)* Muv phenotype. RNAi clones targeting all 656 genes in the worm genome with kinase homology were then screened (Figure 1A). For each gene, ~500 worms were examined and scored for the number of vulva. In this way, we identified 10 genes as suppressors of the Muv phenotype in *let-60(n1046gf)*, and 6 genes as enhancers (Figure 1A). We re-assayed these genes through three confirmatory rounds of screening and identified four consistent enhancers of the *let-60(n1046gf)* Muv phenotype (Figure 1B): *dgk-2/F46H6.2*, *H37N21.1*, *mig-15/ZC504.4* and *hpk-1/F20B6.8*.

dgk-2 encodes a diacylglycerol (DAG) kinase, and cooperation between activating mutations in *RAS* and DAG-activated signalling pathways in mammalian transformation assays is well established (Castagna *et al*, 1982; Nakamura *et al*, 1989). We confirmed that *dgk-2* loss enhances the *let-60(n1046gf)* Muv phenotype using a mutant (null) allele of *dgk-2* (*dgk-2(gk124)*); worms homozygous for *dgk-2(gk124)* showed no obvious phenotype, whereas 100% of *let-60(n1046gf)*; *dgk-2(gk124)* double-mutant worms showed the Muv phenotype due to hyperinduction of vulval progenitor cells (data not shown). In contrast, the mechanism of action for the other three genes was less clear; *mig-15* encodes a Nick-interacting kinase homologue that is known to play a role in cell migration and has been implicated in integrin and WNT signalling (Poinat *et al*, 2002); *hpk-1* encodes a homeo-domain-interacting kinase homologue, and *H37N21.1* encodes an orthologue of the adapter protein *NRBP1*.

gap-1 encodes a member of the *Ras* GTPase-activating protein family and negatively regulates the *let-60* pathway with respect to vulval development. Worms homozygous for a *gap-1* loss-of-function allele (*gap-1(ga133)*) show normal vulval induction (vulval index = 3.0) (Hajnal *et al*, 1997); however, loss of negative regulators of *Ras* signalling such as *lip-1* (Berset *et al*, 2001) can yield a Muv phenotype in these mutants (vulval index > 3.0). RNAi targeting of *H37N21.1* in *gap-1(ga133)* mutants resulted in 17% of worms displaying

the Muv phenotype (vulval index of 3.7); however, no vulval defects were observed when *H37N21.1* was targeted by RNAi in wild-type worms (vulval index of 3.0). This phenotype is indicative of a hyperactivated LET-60 signalling cascade. To further implicate LET-60 signalling, we used a more sensitive assay (*egl-17::cfp*) that reports on the levels of LET-60 signalling, without the *gap-1* mutation in the background, and directly in the vulval cells. Normally, only the descendants of P6.p will express CFP because it receives the highest amount of EGF (LIN-3), but not P5.p or P7.p descendants. We found that worms depleted of *H37N21.1* ectopically express CFP and are therefore displaying excessive LET-60 signalling (Figure 1C). Thus we focused our efforts on *H37N21.1*. *H37N21.1* is an orthologue of *NRBP1* and shows 57.3% amino-acid sequence identity. *NRBP1* and *Nrbp1* from mouse show 99.6% amino-acid sequence identity (Supplementary Figure 1).

Knockdown of *NRBP1* cooperates with activated *Ras* to induce transformation

To determine if *NRBP1* interacts with the *RAS* pathway in mammals, we performed focus formation assays in murine NIH3T3 fibroblasts. Cells stably transfected with *Nrbp1* shRNA did not form foci. In contrast, cells transfected with pBabe-*Ras*^{V12} showed a modest number of transformed foci; however, transfection of pBabe-*Ras*^{V12} into cell lines expressing shRNAs against *Nrbp1* resulted in a significant number of foci (in 3/4 *Nrbp1* shRNAs assayed; Figure 1D). Knockdown of *Nrbp1* protein was confirmed by western blotting (Figure 1E). In agreement with these findings, shRNA-mediated stable knockdown of *NRBP1* in the BJ-ET-st *p53*^{kd}, *p16*^{kd} human fibroblast cell line, which readily transforms following subtle perturbation of the *RAS* pathway or the pathways that regulate the *RAS* signalling cascade (Voorhoeve and Agami, 2003), resulted in a significant increase in the number of transformed colonies in soft agar (in 5/6 *NRBP1* shRNAs assayed; Figure 1F). However, stable repression of *NRBP1* saw no increase in the activation of *RAS* as assayed by western blotting following pull-down using GST-Raf1-BSD (Figure 1G). Thus, just as knockdown of *H37N21.1* in *C. elegans* cooperates with gain-of-function mutations of *let-60*, knockdown of *NRBP1* cooperates with, but does not directly activate, *RAS* in the transformation of mammalian cells in culture. To follow this further, we examined the effect of *Nrbp1* loss *in vivo*.

Generation and analysis of *Nrbp1* conditional and knockout mice

To examine the effect of loss of *Nrbp1* *in vivo*, we created a conditional knockout mouse model. The targeting vector consisted of 9.6 kb of homology to the *Nrbp1* locus, with a *loxP* site inserted in intron 4, and a flrtd PGK-neomycin selection cassette and second *loxP* site inserted in intron 11 (Figure 2A). Correctly targeted E14J ES cells were identified by Southern blot analysis (Figure 2B). Knockout (*Nrbp1*^{+/-}) and conditional (*Nrbp1*^{+/^{lox}) *Nrbp1* alleles were established in mice by breeding male chimeras with Cre and Flp deleters, respectively (Figure 2C). Excision of exons 5–11 disrupts the kinase-like domain of *Nrbp1* and we hypothesised that this would result in nonsense-mediated decay of the remaining transcript.}

Mice heterozygous for the knockout *Nrbp1* allele (*Nrbp1*^{+/-}) were grossly normal at birth and fertile (data

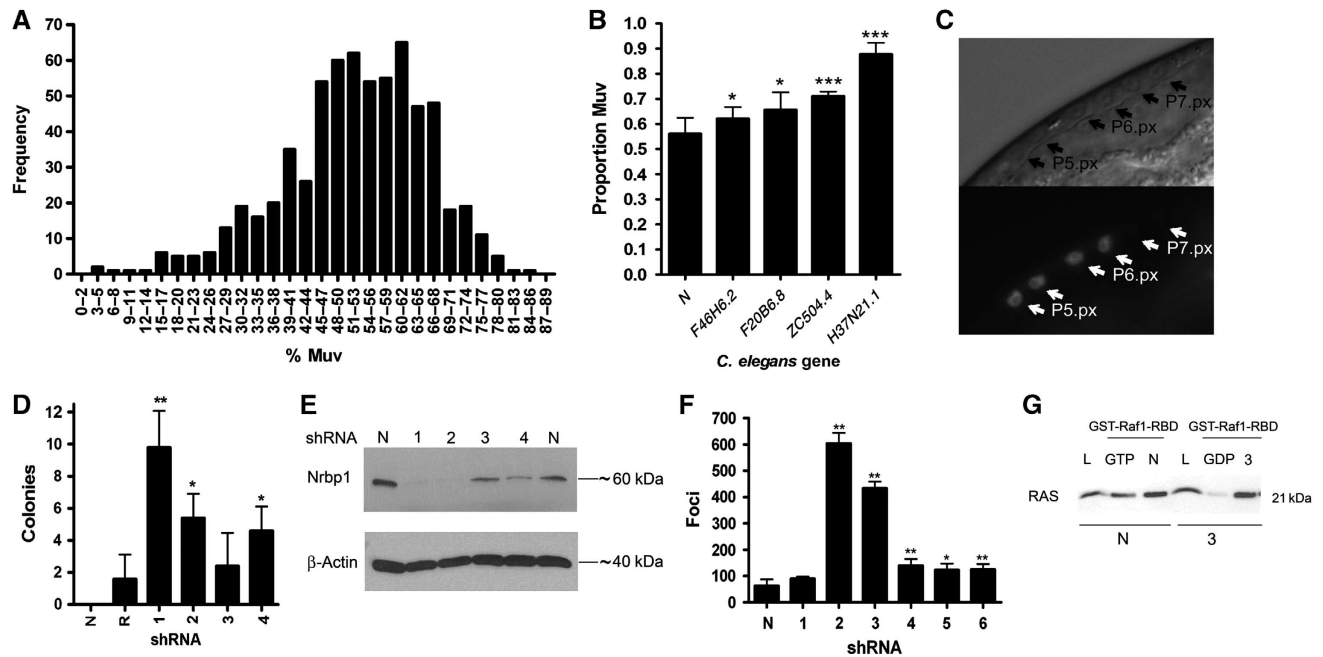


Figure 1 *C. elegans let-60 (n1046gf)* RNAi kinase screen and mammalian *in vitro* transformation analysis. (A) Muv phenotype of *let-60 (n1046gf)* worms after RNAi-mediated knockdown of 656 worm kinase genes. The percentage of animals with a multivulva phenotype is shown. (B) We took the top 2% of genes and performed a second round of screening to identify four robust enhancers of the Muv phenotype. (C) RNAi against *H37N21.1* causes excessive LET-60 signalling in vulval cells. *egl-17::cfp* transgenic worms showing ectopic expression of CFP in P5.p descendants after one cell division (P5.px), which indicates excessive LET-60 signalling. Also shown is the normal CFP expression in the P6.p descendants (P6.px). We observed ectopic expression at a rate of 18% ($n=23$). Top image is light field and bottom image is CFP expression. (D) Histogram of colony numbers from transformants derived from NIH3T3 cells cotransfected with an *Nrbp1* shRNA vector (1–4) and pBabe-*Ras*^{V12} vector. pBabe-*Ras*^{V12} vector alone (R) and empty pBabe vector (N) were used as controls. (E) Western blot analysis of *Nrbp1* knockdown in NIH3T3 cells. (F) Histogram of transformants after BJ-ET-st *p53*^{kd}, *p16*^{kd} cells were transfected with *NRBP1* human shRNA vectors (1–6) or pRS empty vector control (N). (G) BJ-ET-st *p53*^{kd}, *p16*^{kd} transformed colonies transfected with human *NRBP1* shRNA vector 3 were picked, cultured and whole-cell lysates collected for use in pull-down assays using GST-Raf1-BSD. Lysates were separated and visualised using a pan-RAS antibody (L—whole cell lysate, GTP—positive control, GDP—negative control, N—untransfected control cell pull-down, 3—shRNA transformant pull-down). Data are represented as mean \pm s.d.; * $P < 0.05$, ** $P < 0.01$. All shRNA hairpin sequences are available in the Supplementary methods. *** $P < 0.001$.

not shown); however, homozygosity resulted in embryonic lethality at day E7.5 (Supplementary Figure 2). Therefore, loss of *Nrbp1* is not essential for cell viability (since null embryos are able to implant) but defects in or after gastrulation appear to result in embryonic lethality.

Perturbation of proliferation and differentiation of the intestinal epithelium following conditional loss of *Nrbp1*

To establish the phenotypic effects of somatic loss of *Nrbp1*, conditional *Nrbp1* mice (*Nrbp1*^{fllox/fllox} and *Nrbp1*^{fllox/-}) were intercrossed with mice carrying the *Rosa*^{CreERT2} allele (*Rosa*^{CreERT2/CreERT2}), which express Cre-ER^{T2} protein ubiquitously, and at all developmental stages (Hameyer *et al*, 2007). At 7–8 weeks of age, *Nrbp1*^{fllox/fllox} *Rosa*^{CreERT2/+} or *Nrbp1*^{fllox/-} *Rosa*^{CreERT2/+} mice (which showed no phenotypic differences from each other and hereafter are collectively referred to as cKO mice) and *Nrbp1*^{fllox/fllox} *Rosa*^{+/+}, *Nrbp1*^{+/-} *Rosa*^{CreERT2/+} or *Nrbp1*^{fllox/+} *Rosa*^{CreERT2/+} mice (hereafter collectively referred to as control mice) were dosed with tamoxifen (intraperitoneal injection of 4 mg tamoxifen for three consecutive days). cKO mice became moribund as early as 3 days after dosing ($n=11/28$) and 75% died or became moribund by day 9 ($n=21/28$, Figure 2D). In contrast, no control mice died within 174 days post treatment (Figure 2D; $P < 0.0001$).

cKO mice showed macroscopically distended stomachs where food had failed to pass into the intestines and oedematous intestinal tracts with an abnormal mucosal appearance. Histopathological analysis of the brain, kidneys, skin, thymus, heart, pancreas, lungs, uterus/testis and spleen of control and cKO mice revealed no abnormalities. However, cKO mice showed zone 3 hydropic changes in their livers, indicative of malnutrition (data not shown), and the intestines showed a complete loss of architecture, including reduced numbers of differentiated cells, cells showing dysplastic nuclear atypia, widespread crypt elongation by primitive looking cells and reduced villous length (Figure 2E). An increased level of crypt fission was also observed (Figure 2F). To examine the expression pattern of *Nrbp1* in the intestine, we performed *in situ* hybridisation (ISH) analysis using a probe specific to the conditionally deleted region of *Nrbp1*. In control intestines, expression of *Nrbp1* was found to be highest in the Paneth, enteroendocrine and precursor goblet cell lineages; however, *Nrbp1* expression was also found in the crypt and to overlap with the *Lgr5* and *Olfm4*-positive stem cells (Supplementary Figure 3). To confirm the specificity of the *Nrbp1* *in situ* probe, we analysed tamoxifen-treated cKO tissues and as expected little or no *Nrbp1* expression was observed (Figure 2G). Similarly, western blotting showed a downregulation in *Nrbp1* protein levels in the intestine of tamoxifen-treated cKO mice (Figure 2G).

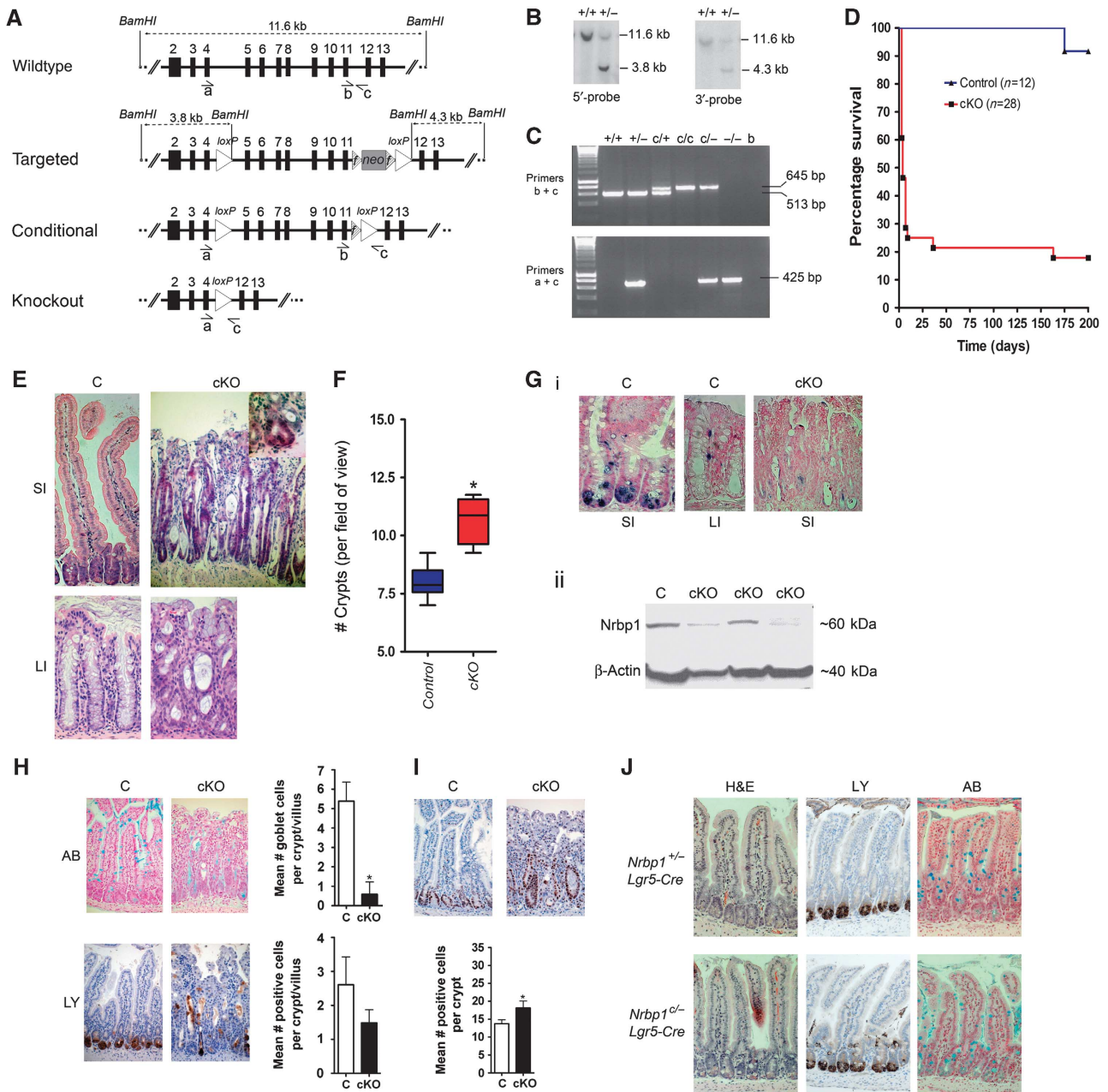


Figure 2 Generation and characterisation of *Nrbp1* knockout mice. **(A)** Schematic representation of the *Nrbp1* locus, along with targeted, conditional and knockout *Nrbp1* alleles. The PGK-neomycin selection cassette (*neo*) is flanked by *Frt* sites (striped triangles). Open triangles indicate *LoxP* sites for conditional deletion of exons 5–11. **(B)** Confirmation of correct targeting was performed by Southern blot analysis of *Bam*HI-digested DNA; The wildtype band for both 5'- and 3'-probes was 11.6 kb and the targeted band was 3.8 and 4.3 kb, respectively. **(C)** Subsequent genotyping was performed by PCR, using either primers 'b/c' to detect the wild-type and conditional allele, or primers 'a/c' to detect the knock out allele. **(D)** Survival curve of *Nrbp1*^{fllox}, *Rosa*^{CreERT2/+} (cKO) mice and controls after intraperitoneal dosing with 3 mg tamoxifen per day for 3 days. **(E)** H&E staining of the SI (small intestine) and LI (large intestine) from C (control; *Nrbp1*^{+/-} *Rosa*^{CreERT2/+} or *Nrbp1*^{fllox/+} *Rosa*^{CreERT2/+}) and cKO (*Nrbp1*^{fllox/fllox} *Rosa*^{CreERT2/+} or *Nrbp1*^{fllox/-} *Rosa*^{CreERT2/+}) mice at 5–7 days post tamoxifen treatment showing crypt elongation by primitive looking cells ($\times 200$ magnification). Inset: cKO intestines show evidence of crypt fission. **(F)** cKO mouse intestines had more crypts per field of view than C intestines at 4–5 days post dosing. **(G)** (i) ISH analysis using probe specific to *Nrbp1* in the SI (small intestine) and LI (large intestine) of C mice (control; $\times 400$ magnification) and the SI of cKO mice ($\times 200$ magnification) at 5 days post tamoxifen treatment, showing reduction of *Nrbp1* expression levels in cKO tissue. **(G)** (ii) Western blot analysis of intestinal tissue harvested from C and cKO mice at 5 days post treatment with 1 mg tamoxifen for 4 days shows a reduction of Nrbp1 protein levels. β -Actin levels used as a control. **(H)** Histological and immunohistochemical analysis showing cKO mouse intestines had fewer goblet cells (as determined by Alcian blue staining) and an altered distribution of Paneth cells (as determined by lysozyme staining) compared to C mice at 4–5 days post dosing. **(I)** cKO mice had more proliferating cells (as determined by Ki67 immunopositivity) than C intestines at 4–5 days post dosing. Data are represented as mean \pm s.d.; $*P < 0.05$. **(J)** Histological and immunohistochemical analysis of the small intestines of 7–8-week-old *Nrbp1*^{-/-}*Lgr5*-EGFP-IRES-CreER^{T2} and *Nrbp1*^{-/-}*Lgr5*-EGFP-IRES-CreER^{T2} control mice at 4–5 post dosing with 1 mg tamoxifen for 3 days. Data are represented as mean \pm s.d. ($n = 6$ per genotype). Stem cell-specific deletion of *Nrbp1* resulted in abnormal paneth cell localisation and granulisation, and abnormal goblet cell production ($\times 200$ magnification; haematoxylin and eosin, H&E; anti-lysozyme antibody, LY; Alcian blue, AB). $**P < 0.01$, $***P < 0.001$.

Histological analysis of each of the cell types that constitute the intestinal epithelium, revealed most notably a marked decrease in the number of Alcian Blue positive goblet cells, an altered distribution of Paneth cells (Figure 2H) and reduced enteroendocrine cells (Supplementary Figure 3). In addition, expression of the proliferation marker Ki67 and the number of mitotic figures were significantly increased, while expression of the apoptotic marker cleaved caspase 3 was not significantly changed (Figure 2I, Supplementary Figure 3). To further investigate the phenotypic effect of *Nrbp1* deficiency specifically within the intestinal stem cell compartment, we utilised the *Lgr5-EGFP-IRES-CreER^{T2}* knock-in mouse, which expresses CreER^{T2} specifically within the *Lgr5*-positive stem cell compartment with recombination occurring in a sporadic and low-penetrant fashion (<10% intestinal stem cells) upon tamoxifen treatment (Barker *et al*, 2007; Barker *et al*, 2009). Immunohistochemical analysis of small intestines from *Nrbp1*^{-/-}*Lgr5-EGFP-IRES-CreER^{T2}*⁺ mice at 5 days post tamoxifen treatment (intraperitoneal dosing of 1 mg/ml tamoxifen for 3 days) showed a similar phenotype to cKO mice, albeit to a lesser extent due to the very low level of recombination, with Paneth cells displaying abnormal localisation and granularisation, and abnormal goblet cell production (Figure 2J).

Together, these data indicate that loss of *Nrbp1* protein in the adult intestines of mice causes aberrant proliferation of progenitor-like cells in the crypts and increased crypt fission, which profoundly affects the normal programmes of cellular differentiation and localisation along the crypt-villus axis. These features are similar to several mouse models engineered to perturb the WNT pathway (Battlle *et al*, 2002; Sansom *et al*, 2004; Madison *et al*, 2005; Finch *et al*, 2009).

Expression profiling of *Nrbp1*-deficient intestinal cells

To evaluate the role of loss of *Nrbp1* in intestinal homeostasis, we performed microarray expression profiling on small intestinal epithelial cells from tamoxifen-dosed control and cKO mice. For these experiments the Cre driver used was *Rosa^{CreERT2/+}*. The expression of 3331 genes was significantly altered ($P < 0.01$ to 2 decimal places between these groups (Supplementary Table 1). Interestingly, a number of WNT-responsive genes showed significantly increased expression in cKO mice compared with controls, including *Ccnd1*, *Cd44*, *Mmp7*, *Sox9* and *Tnfrs12a*.

To validate the expression arrays, we examined the expression of a number of WNT-responsive genes by quantitative RT-PCR (qRT-PCR). Expression of *Cd44*, *c-Myc* and *Ccnd1* were upregulated more than three-fold in the intestinal epithelium of cKO mice compared with controls (Figure 3A). Further examination of WNT target genes by immunohistochemistry and ISH analysis of the small intestines revealed increased staining for *c-Myc*, *Sox9*, *Mmp7* and *Lgr5* in cKO mice compared with controls (Figure 3B). In addition, cKO mice showed a widespread increase in pErk nuclear positivity and β -catenin staining in the mucosa that matched the upward spread of crypt progenitor-like cells (Figure 3C). In addition, although the clearest signature was for the WNT pathway, we note that a number of other signalling pathways were also significantly altered—for example, expression analysis of the *Notch* genes revealed that *Notch3* and *Notch4* were both significantly overexpressed

and this in turn lead to an increase in *Hes1* expression (Supplementary Figure 4).

We next compared our differentially expressed gene set to gene expression signatures of genetic and chemical perturbations using the Molecular signatures database MSigDB Version 2.5 (<http://www.broadinstitute.org/gsea/msigdb/index.jsp>) (Subramanian *et al*, 2005). There was a striking overlap ($P = 5.89 \times 10^{-23}$ and $P = 5.5 \times 10^{-47}$) with genes down-regulated at 4 or 5 days following conditional deletion of adenomatous polyposis coli (*Apc*) in the mouse intestine (Sansom *et al*, 2004) (Supplementary Figure 5). Similarly, there was a significant overlap between genes that were upregulated upon loss of either *Apc* or *Nrbp1* ($P = 0.007$ (5 days) $P = 6.2 \times 10^{-6}$ (4 days); Supplementary Figure 5), suggesting that similar changes to the programmes of gene expression occur following loss of either gene. These expression changes may also reflect changes in the constitution of the cells that make up the intestinal epithelium.

To further investigate the role of *Nrbp1* within the intestine, we grew *Nrbp1* cKO and control crypts *ex vivo*. Using adenoviral cre infection of organoid cultures to delete *Nrbp1*, we observed decreased organoid budding and organoid dis-organisation (Supplementary Figure 6). After long-term culture of these organoids they eventually regained the ability to bud, presumably due to the outgrowth of non-recombined cells (Koo *et al*, 2011). On removal of R-spondin from early cultures all crypts of all genotypes died, indicating that *Nrbp1* null crypts are still dependant on Wnt signalling.

Nrbp1 interacts with Elongin BC E3 ubiquitin ligase complex

To further explore possible roles for *Nrbp1* within mammalian cells, we performed tandem affinity purification followed by mass spectrometric analysis using a FTAP-tagged human *NRBP1* cDNA expression plasmid in mouse ES cells (E14J; 129P2/Ola). Five proteins were shown to bind strongly to NRBP1, including Tceb1 (Elongin B), Tceb2 (Elongin C), Tsc22d2, Tsc22d4 and Sall4 (Supplementary Table 2). To validate these results, we performed single affinity purifications from human HEK293 cells expressing the same FTAP-tagged human *NRBP1* cDNA. We were able to recover TCEB1, TCEB2, TSC22D2 and TSC22D4, among others. SALL4 was not recovered, most likely due to the stem cell-specific expression of SALL4; we therefore confirmed that Sall4 binds to *Nrbp1* in mouse ES cells by coimmunoprecipitation (Figure 4A). We also confirmed binding of *Nrbp1* to Elongin B and Elongin C by coimmunoprecipitation (Figure 4B). Since ELONGIN B and the TSC22s have been shown to bind to NRBP1, and NRBP1 carries both a functional Elongin BC-binding motif (BC-Box) and a CUL5-binding site (Supplementary Figure 1) (Rual *et al*, 2005; Mahrouf *et al*, 2008; Gluderer *et al*, 2010), we hypothesised that it may function as a substrate recognition subunit of a Cul5 E3 ligase complex. Indeed, expression of NRBP1, ELONGIN B, ELONGIN C and CUL5 in HEK293 cells allowed coimmunoprecipitation of CUL5 with NRBP1, only when ELONGIN B and ELONGIN C were present in the lysate (Figure 4B). This is in contrast to a previous report suggesting that NRBP1 is not part of a complex with CUL5 (Mahrouf *et al*, 2008). To further investigate if NRBP1 could be functioning within an Elongin BC E3 ubiquitin ligase complex, we performed western blot and immunohistochemical analysis on intestinal tissue from tamoxifen-treated cKO mice and found a significant increase

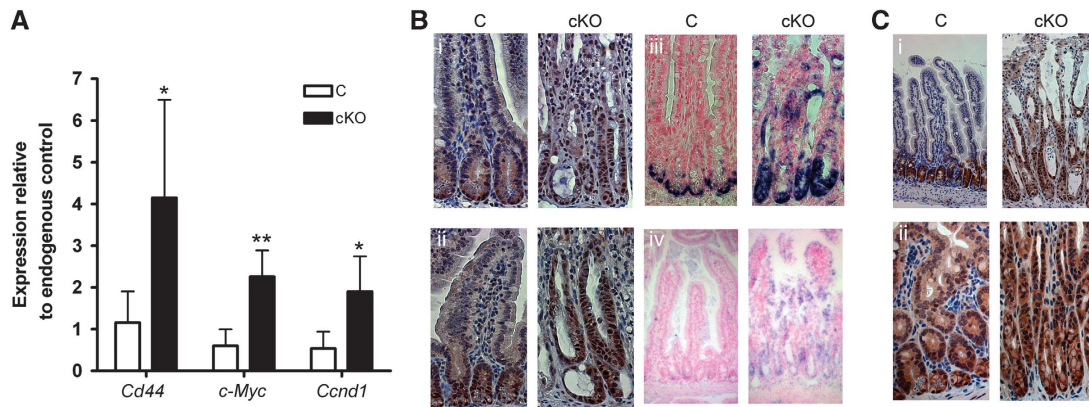


Figure 3 Expression analysis of conditional *Nrbp1* mice. (A) qRT-PCR analysis of the WNT target genes, *Cd44*, *c-Myc* and *Ccnd1* in the intestine of cKO and C mice at 4–5 days post tamoxifen administration. (B) Immunohistochemical (i, ii) and *in situ* analysis (iii, iv) of small intestines from C and cKO mice at 7–9 days post tamoxifen treatment indicating loss of *Nrbp1* causes an increase in (i) *c-Myc* ($\times 400$ magnification), (ii) *Sox9* ($\times 400$ magnification), (iii) *Mmp7* ($\times 400$ magnification) and (iv) *Lgr5* ($\times 200$ magnification). (C) Immunohistochemical analysis of small intestines from C and cKO mice at 7–9 days post tamoxifen treatment show increased expression of (i) pErk ($\times 200$ magnification), but no obvious increase in (ii) nuclear Ctnnb1 signal ($\times 400$ magnification). * $P < 0.05$, ** $P < 0.01$.

in both Tsc22d2 and Sall4B protein levels compared to controls (Figures 4C and D and Supplementary Figure 7) suggesting that *Nrbp1* may have a role in the turnover or accumulation of these proteins. It is, however, important to note that as yet we have been unable to functionally link *Nrbp1* to the ubiquitination of these proteins. Intriguingly, overexpression of SALL4 has been shown to play a role in regulating the WNT pathway in the haematopoietic system through a direct physical interaction with β -catenin (Ma *et al*, 2006). Here, we show that knock-down of *NRBP1* or overexpression of SALL4 in HCT-116 human colon cancer cells results in an upregulation of WNT reporter activity (Figure 4E) suggesting a direct link between *NRBP1* and the WNT pathway through SALL4, an avenue we are currently investigating further.

Nrbp1* is a tumour suppressor *in vivo

Given *Nrbp1* proficiency is vital for intestinal homeostasis and loss of *Nrbp1* cooperates with oncogenic *Ras* and can modulate Wnt signalling, we hypothesised that *Nrbp1* may be a tumour suppressor *in vivo*. In our initial survival analysis (Figure 2D), 18% ($n = 5$) of cKO mice survived the acute intestinal phenotype associated with loss of *Nrbp1*, and histological analysis of their intestines revealed no abnormalities. This suggested incomplete recombination of the *Nrbp1* allele and intestinal regeneration by the surviving cells (Muncan *et al*, 2006). To generate a cohort of mice for tumour watch, we treated 7–8-week-old control and cKO mice with a lower dose of tamoxifen (intraperitoneal dose of 1 mg tamoxifen for four consecutive days) and placed them on tumour watch. cKO mice showed significantly reduced survival compared to controls, which was associated with an increased incidence of tumorigenesis, including lymphomas/leukaemias and solid tumours ($P = 0.006$; Figure 5A–C). Interestingly, 38% (6/16) of the cKO mice displayed gastrointestinal tract tumours, specifically four were adenomas with high-grade dysplasia and two were invasive adenocarcinoma (5/6 tumours were located in the caecum; Figure 5B). *In situ* analysis of these tumours confirmed loss or reduction in *Nrbp1* RNA levels (Figure 5Di), and immunohistochemical analysis showed widespread nuclear *c-Myc* and pErk staining (Figure 5Dii–iv), analogous to

the staining patterns identified in the ‘early *Nrbp1*-null phenotype’. Taken together, these data are all consistent with a role for *Nrbp1* as a tumour suppressor gene *in vivo*.

Reduction in *Nrbp1* expression is seen in a wide variety of human tumours and correlates with poor prognosis

To further explore the association of *NRBP1* loss in cancer, we performed expression analysis on a wide variety of human tumour types (including leukaemia, lymphoma, colorectal, breast, brain, oesophageal, renal cell, prostatic and lung cancers) and found significantly reduced *NRBP1* expression levels in many of these tumour types when compared with relevant control tissues ($P < 0.01$; Figure 6A). As lung adenocarcinoma showed the most significant difference in *NRBP1* expression levels between normal and tumour tissues, and survival analysis data was available, we examined the relationship between *NRBP1* expression and survival and found that low *NRBP1* expression strongly correlated with a poor prognosis ($P = 0.008$; Figure 6B).

Discussion

Cancer is a multistep process that requires extensive synergy between oncogene activation and tumour suppressor gene loss. Many oncogenes are key components of highly conserved signalling pathways, and genetic screens in model organisms including *Drosophila* and *C. elegans* have identified oncogene orthologues in the EGF, WNT, NOTCH and TGF β pathways, among others. However, such screens have yielded few orthologues of tumour suppressor genes. In this paper, we employed the power of RNAi screening in *C. elegans* to identify candidate tumour suppressor genes by screening for genes that enhanced developmental defects due to gain-of-function mutations in *Ras*. Importantly, we found that loss of *H37N21.1*, the worm orthologue of *NRBP1*, enhanced the effect of gain-of-function mutations in *Ras* suggesting that it may act as a tumour suppressor gene in mammals.

NRBP1 is a highly conserved adaptor protein that we show is required for early mouse embryonic development. In mammalian *in vitro* systems, we have shown that together with oncogenic RAS, *NRBP1* knockdown leads to an increase in transformation; however, *NRBP1* loss does not appear to

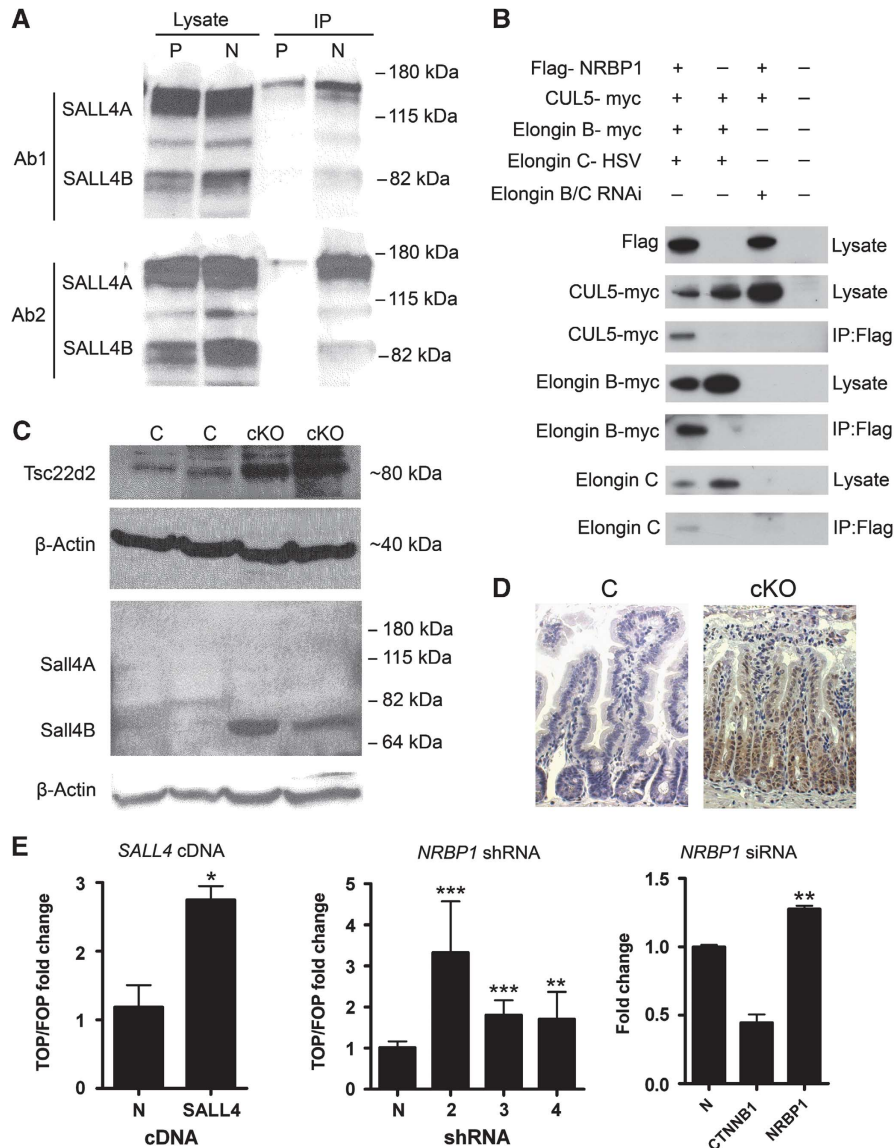


Figure 4 NRBP1 interacts with components of the Elongin BC E3 ubiquitin ligase complex. (A) Immunoprecipitation with anti-Flag antibody of mouse ES cells carrying either Flag-tagged *NRBP1* cDNA expression plasmid (N) or Flag-tagged *Phactr2* cDNA expression plasmid (P) as a control, followed by western blotting with one of two different anti-Sall4 antibodies (Ab1 and Ab2), showed coprecipitation of both Sall4 isoforms with Nrbp1 and not the control. In mouse ES cells, Sall4 has been shown to run at 85 and 140 kDa. (B) Immunoprecipitation of CUL5 and other members of the ubiquitination machinery with NRBP1 from HEK293 cells. (C) Western blot analysis with anti-Tsc22d2 antibody, anti-Sall4 and anti-β-Actin control antibody of intestinal tissue harvested at day 5 from cKO (*Nrbp1^{flox} Rosa^{CreERT2/+}*) or C (control; *Nrbp1^{flox} Rosa^{+/+}*) mice treated with 1 mg tamoxifen for 4 days. In somatic cells, Sall4 has been shown to run at 66 and 113 kDa. (D) Immunohistochemical analysis of Sall4 in the intestinal tissue from C (control; *Nrbp1^{flox} Rosa^{+/+}*) and cKO (*Nrbp1^{flox} Rosa^{CreERT2/+}*) mice at 4–5 days post tamoxifen treatment showing elevated levels of Sall4. (E) Transcriptional activation of *TCF/LEF* measured using the dual luciferase assay (TOP/FOP) in HCT-116 colon cancer cells transfected with a *Sall4* cDNA plasmid (left panel) or an *NRBP1* shRNA construct (middle panel). N refers to an empty vector control. Transcriptional activation of *TCF/LEF* was also measured by siRNA-mediated knockdown of NRBP1 in SW180 WNT reporter cells (right panel). Knockdown of CTNNB1 was used as a control. * $P < 0.05$, ** $P < 0.01$, *** $P < 0.001$.

affect RAS signalling directly suggesting that other pathways must modulate RAS activity following NRBP1 loss. To investigate the function of *Nrbp1* *in vivo*, we constructed a conditional knockout mouse model. Two somatic phenotypes were discerned depending on the pattern of *Nrbp1* disruption. First, there was an ‘early intestinal phenotype’ at 4–9 days post tamoxifen dosing. This phenotype consisted of expansion of crypt progenitor-like cells with aberrant proliferation in elongated crypts and increased crypt fission, together with abnormal differentiation and localisation of cells along the crypt–villus axis. Ultimately this phenotype led to abnormal intestinal function, malnutrition and the death of over 80%

mice by 5–10 days (Figure 2). The intestinal epithelia of these mice showed several similarities to mouse models engineered to perturb the WNT pathway (Batlle *et al*, 2002; Sansom *et al*, 2004; Madison *et al*, 2005; Finch *et al*, 2009). Interestingly, the phenotype also shows a striking similarity to a model in which the POU-family transcription factor *Oct4* was overexpressed in the intestine (Hochedlinger *et al*, 2005). We tentatively speculate that *Nrbp1* regulates Sall4 levels through its role in an Elongin BC E3 ubiquitin ligase complex and thus suggest that the intestinal phenotype of the *Nrbp1* cKO mice may possibly be due to increased levels of Sall4 influencing cell fate by perturbing the WNT pathway, which tips the balance of

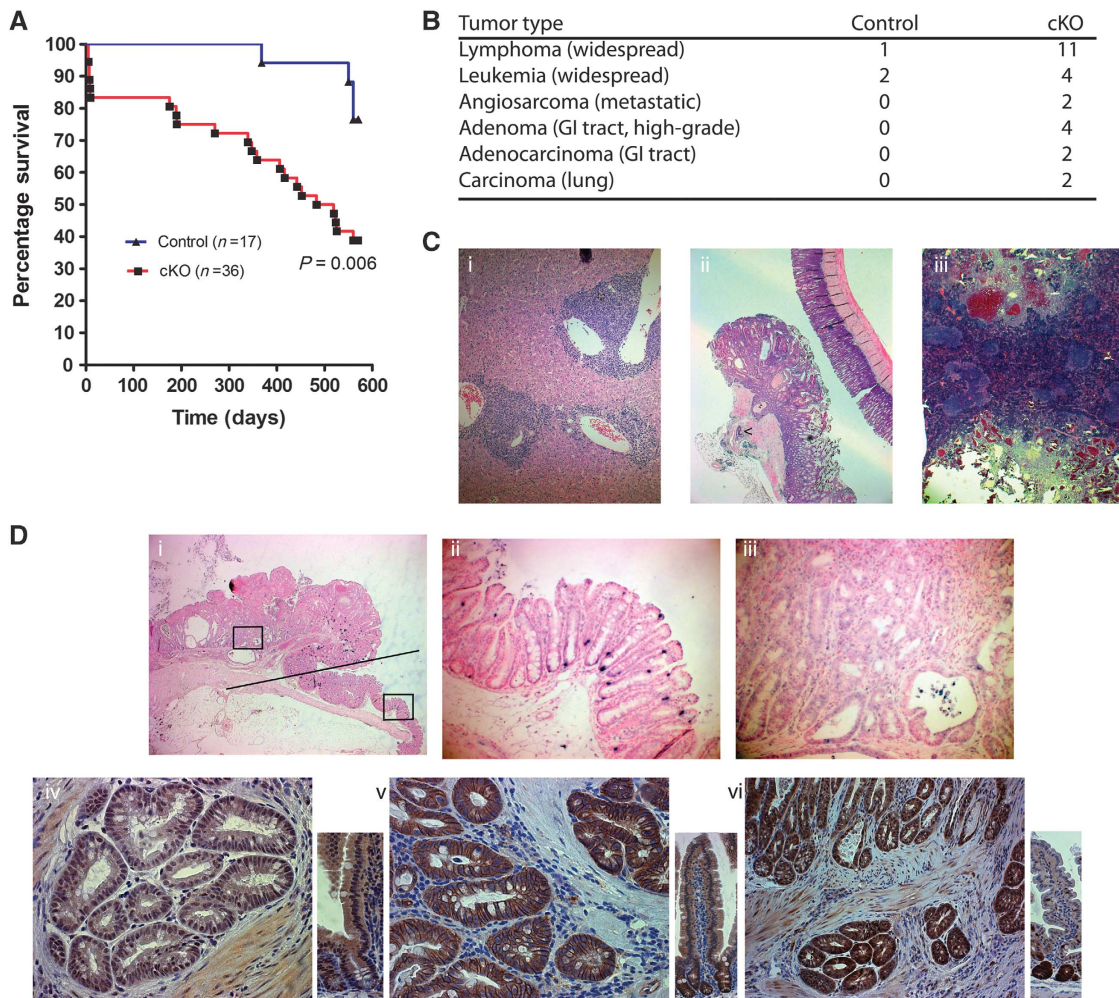


Figure 5 *Nrbp1* is a tumour suppressor *in vivo*. (A) Survival analysis of cKO ($Nrbp1^{flox/Rosa^{CreERT2/+}}$) and control mice ($Nrbp1^{flox/+} Rosa^{CreERT2/+}$ and $Nrbp1^{flox/flox} Rosa^{+/+}$) after treatment with 1 mg tamoxifen per day for 4 days. Animals became moribund and were culled as a result of either an ‘early *Nrbp1* loss phenotype’ (animals <10 days post treatment) or when they developed macro/microscopically visible tumour(s) (animals >10 days post treatment). (B) Table provides a summary of the tumour types found in the mice (some animals had more than one type of tumour). (C) H&E staining of tissues from cKO mice showing (i) widespread lymphoma in the liver ($\times 100$ magnification), (ii) invasive colorectal adenocarcinoma ($\times 250$ magnification) and (iii) high-grade angiosarcoma in the spleen ($\times 250$ magnification). (D) ISH analysis of *Nrbp1* in a colorectal lesion from an $Nrbp1^{flox/Rosa^{CreERT2/+}}$ mouse shows (i) a tumour area left of the black line, and normal colonic tissue right of the black line ($\times 25$ magnification), with the lower box enlarged in (ii) and the upper box enlarged in (iii), showing reduced *Nrbp1* expression levels in tumour tissue ($\times 200$ magnification). Immunohistochemical analysis of an invasive colorectal adenocarcinoma from an $Nrbp1^{flox/Rosa^{CreERT2/+}}$ mouse showing significant strongly positive staining with (iv) c-Myc ($\times 400$ magnification) and (vi) pErk ($\times 200$ magnification) antibodies, but (v) no increased nuclear Ctnnb1 signal ($\times 400$ magnification).

progenitor cells from differentiation to proliferation. As yet, however, we have been unable to conclusively prove this functional link. Furthermore, although we were able to pull-down complexes containing components of the ubiquitination machinery and *Nrbp1*, we have been unable to conclusively prove a role for *Nrbp1* in protein turnover. Indeed, the data we have collected on *Nrbp1* suggest that it may have pleiotropic effects on several pathways.

Most of the mice which survived this ‘early intestinal phenotype’ went on to develop a wide range of tumours, including intestinal adenomas in 38% of mice, a third of which had advanced to invasive intestinal adenocarcinoma, as well as lung adenocarcinomas, lymphomas, leukaemias and angiosarcomas, with significantly reduced survival. Thus, *Nrbp1* acts as a tumour suppressor gene *in vivo* with *Nrbp1* loss resulting in a tendency to intestinal adenoma/adenocarcinoma and lymphoma/leukaemia formation

(Figure 5). Analysis of human cancer expression datasets showed that *NRBP1* is downregulated in a range of tumour types, and that in lung adenocarcinomas low *NRBP1* expression is associated with a poorer prognosis (Figure 6). It is intriguing to note that although we were able to recapitulate the acute intestinal phenotype associated with loss of *Nrbp1* by expressing *CreER^{T2}* specifically in *Lgr5⁺* stem cells (Figure 2J), and that loss of *Nrbp1* activates the WNT pathway (Figure 3), we have not observed intestinal polyposis or tumourigenesis in $Nrbp1^{-/-} Lgr5-EGFP-IRES-CreER^{T2/+}$ mice up to 100 days (data not shown). This may be because of the modest activation of the WNT pathway we observed and because fewer cells underwent recombination using the *Lgr5-EGFP-IRES-CreER^{T2}* allele. In both models of Cre recombination and in *ex vivo* crypt culture, it appears that selection against *Nrbp1* loss occurs suggesting that by itself *Nrbp1* is unlikely to be an initiating event in colorectal cancer,

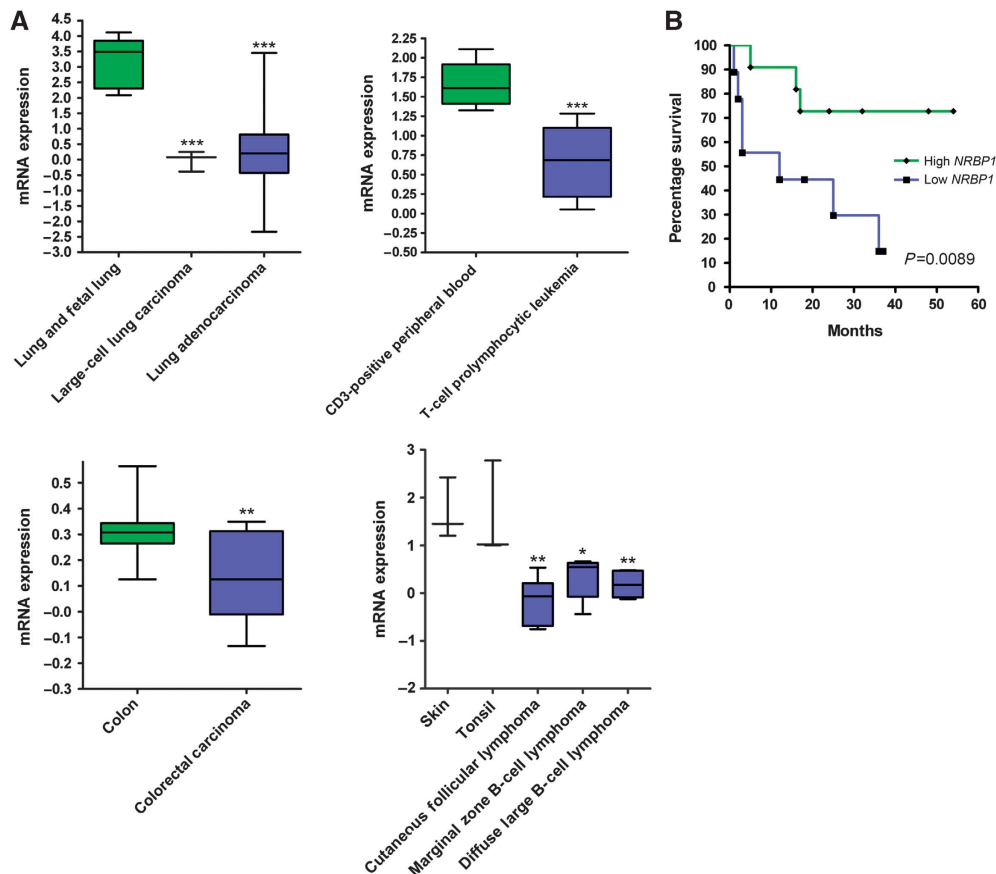


Figure 6 Associations of altered *NRBP1* expression with human cancers. **(A)** Expression analysis of *NRBP1* in human large-cell lung carcinoma, lung adenocarcinoma, T-cell prolymphocytic leukaemia, colorectal carcinoma, cutaneous follicular lymphoma, marginal zone B-cell lymphoma and diffuse large B-cell lymphoma compared to relevant normal tissues. **P* < 0.05, ***P* < 0.01 and ****P* < 0.001. **(B)** Survival analysis of patients with lung adenocarcinoma expressing either high (green) or low (blue) *NRBP1* expression levels.

instead cooperating mutations are likely to be required for tumorigenesis.

We have shown that *NRBP1* interacts with *ELONGIN B* and *C* and *CUL5*, which are components of an E3 ubiquitin ligase complex. The Elongin BC complex is a heterodimer composed of *ELONGIN C* and *ELONGIN B*, that was initially identified as a positive regulator of RNA polymerase II elongation factor *ELONGIN A* (Reines *et al*, 1999). A more recognised role of Elongin BC is within the tumour suppressor complex together with the von Hippel-Lindau (*VHL*) protein, which targets the transcription factor hypoxia inducible factor-1 α for ubiquitination (Duan *et al*, 1995; Kibel *et al*, 1995). Interaction of the Elongin BC complex with proteins such as *VHL* and suppressors of cytokine signalling (*SOCS*) depends on binding to a ~10 amino-acid degenerate sequence motif, referred to as the BC-box, which has the consensus sequence of [(A/P/S/T)-L-X₃-(C/S/A)-X₃-(A/I/L/V)], a motif also present in *NRBP1* (Supplementary Figure 1). The BC-box-containing protein mediates substrate binding and specificity, while Elongin BC functions as an adapter that links it to a Cullin/Rbx module that functions to recruit and activate an E2 ubiquitin conjugating enzyme for ubiquitylation of substrates. In addition to *VHL* and *SOCS*, a number of novel BC-box proteins have been shown to assemble with Cullin/Rbx and therefore it has been predicted that a larger family of *ELONGIN BC*-based E3 ubiquitin ligases exists (Kamura

et al, 2001). We therefore suggest that *NRBP1* is involved in substrate recognition within a RING-type E3-ligase complex to enhance the ubiquitin-mediated degradation of proteins. As yet, however, confirming this hypothesis has proved elusive. Potential substrates of *NRBP1* could include *TSC22d2* and *SALL4*, which we show bind strongly to *NRBP1* and both show increased protein levels *in vivo* when *Nrbp1* is deleted in the mouse (Figure 4). *Sall4* is a transcription factor that plays an essential role in maintaining embryonic stem cell pluripotency and self-renewal (Warren *et al*, 2007). Interestingly, overexpression of *SALL4* has been shown to cause aberrant activation of the WNT pathway in myelodysplastic syndromes (Shuai *et al*, 2009), and *SALL4* expression has recently been linked to gastric cancers (Ushiku *et al*, 2010). Furthermore, *sem-4*, the *C. elegans* orthologue of *SALL4*, promotes vulval cell fate determination. *TSC22d2* is a member of the *TSC22* (TGF β -stimulated clone 22) family of putative transcription factors that is activated by TGF β 1 receptor signalling (Jay *et al*, 1996). *Tsc22* has been shown to be expressed at sites of epithelial mesenchymal interactions from the early stages of mouse development (Dohrmann *et al*, 1999). Indeed when we performed ISH analysis of intestinal tissue from *Nrbp1* cKO mice, *Tsc22d1* and *Tsc22d4* were both strongly expressed in the pericryptal fibroblasts while *Tsc22d2* was expressed primarily in the crypt regions (Supplementary Figure 6) suggesting a possible role in signalling from the intestinal

mesenchyme to cryptal cells. The TSC22 protein family is conserved between humans and *C. elegans*, but the function of these proteins has been difficult to determine due to differences in isoforms, redundancy, synergistic and/or antagonistic functions (Gluderer *et al*, 2010). Much of the work on these proteins has been carried out in *Drosophila*, and the data have suggested genetic interactions with the fly orthologues of BMP, WNT, HH, NOTCH and components of the EGFR signalling pathway (Treisman *et al*, 1995; Dobens *et al*, 2000; Dobens *et al*, 2005). Furthermore, in this system the fly orthologue of NRBP1 (Madm) and the long isoform of TSC22, *Bunched* (*bunA*), have been shown to directly bind, and loss of either protein leads to similar growth phenotypes. It is interesting to note that TSC22D1 has been shown to be highly induced by oncogenic RAS expression and together with TSC22D4 regulate oncogene-induced senescence (Homig-Holzel *et al*, 2011).

In conclusion, using a novel combination of RNAi screens in worms together with detailed follow-up experiments in mouse and human cells, we show that *NRBP1* is a tumour suppressor that plays a critical role in intestinal cell homeostasis. Crucially, *NRBP1* levels are reduced in a wide variety of human tumours and, furthermore, reduced *NRBP1* levels in lung cancer correlates with a poor prognosis.

Materials and methods

C. elegans RNAi

Nematode strains used in this work were provided by the Caenorhabditis Genetics Centre. Screening was performed at 16 °C in 12-well plates using 715 bacterial RNAi clones (Supplementary Table 3) to target 656 transcripts with kinase or kinase-like motifs from the Ahinger library (Kamath *et al*, 2003). Bacterial RNAi feeding strains were grown overnight in 2TY plus 100 µg/ml ampicillin at 37 °C and spotted onto plates containing LB, 100 µg/ml ampicillin and 4 mM IPTG. Approximately 10 L4 staged worms were dispensed to the first well of each row and grown for 72 h, after which 1 adult worm was moved to a separate well and left overnight before removal. Embryos were left to mature for at least 72 h and scored for Muv in 100–200 animals in triplicate by visual inspection using a dissecting microscope. Muv was scored in comparison to the phenotype of the worm strain alone. The top and bottom 2% of genes were retested in two separate confirmatory rounds of screening. For *egl-17::cfp* assays, L3 animals were mounted and examined for persistent expression of *egl-17::cfp* prior to L4.

Cell culture, transformation assays and luciferase assays

All cell lines (NIH3T3, HEK 293, BJ-ET-st *p53^{kd}, p16^{kd}*, SW480 and HCT-116) were cultured in DMEM supplemented with 10% fetal bovine serum and glutamine/penicillin/streptomycin. For focus formation assays, NIH3T3 cells were transfected using lipofectamine (Invitrogen) with 200 ng of pBabe-Ras^{V12} plasmid DNA together with 200 ng of pRS shRNA plasmid DNA designed against *Nrbp1* (the sequence of shRNA hairpins is provided in the Supplementary methods) or an empty vector control. Cells were seeded at 1×10^5 per 6-cm plate and fed every 4 days for 2 weeks and then stained with methylene blue and foci were counted. Each experiment involved five replicate transfections performed on three separate occasions. BJ-ET-st *p53^{kd}, p16^{kd}* soft agar assays were performed as described previously (Voorhoeve and Agami, 2003) with human pRS shRNAs (provided in Supplementary methods), which were modified to introduce a blasticidin resistance cassette driven by the PGK promoter. Data were statistically analysed using the Mann-Whitney *U*-test. Luciferase assays were performed in 24-well plates with 7.5×10^5 HCT-116 or HEK 293 cells. Cells were cotransfected using lipofectamine with either 200 ng *NRBP1* shRNA vectors or empty vector in combination with either 150 ng M50 Super 8x TOPFlash or M51 Super 8 × FOPFlash and 50 ng Renilla (pRL-SV40) plasmid. At 72 h after transfection, cells were lysed in 100-µl passive lysis buffer, and the dual luciferase assay performed

according to the manufacturers protocol (Promega). The relative luciferase activity was calculated against Renilla activity. Each shRNA was assayed in experiments involving six replicates and these experiments were performed on at least two separate occasions. Data were statistically analysed using ANOVA. CellSensor assays were performed in 96-well plates with 2.4×10^4 SW480 cells. Cells were transiently transfected with 20 nm siRNA (Dharmacon) using Lipofectamine RNAimax (Invitrogen). At 72 h after transfection FRET read-out was measured using beta-lactamase loading solution (Invitrogen) by standard procedures. Data were statistically analysed using ANOVA. *Ex vivo* crypts were isolated from *Nrbp* cKO and control mice small intestine by incubating in 2 mM EDTA in PBS. Crypt cultures were grown in Matrigel (BD biosciences) and provided with Advanced DMEM/F23 (Invitrogen) supplemented with N2 (Invitrogen), B27 (Invitrogen), EGF (Peprotech), NOGGIN (Peprotech) and mR-Spondin (R&D Systems) (Sato *et al*, 2009). Adenoviral infection of crypts was performed by mechanically separating crypts away from Matrigel and incubating with Adeno-Cre or Adeno-GFP (as a control) virus at 37 °C for 3–4 h before re-plating in Matrigel. GFP expression was seen in ~80% of cells the day after infection.

Mice

To generate the *Nrbp1* targeting vector, DNA fragments for the 5'- and 3'-homology arms were amplified from bMQ-76E6 BAC (Adams *et al*, 2005) by PCR using the following primers: Capture arms1F—AA AAAAAAAAAAGAGCTCCTGGTCTCTAGTTTATGATTCATG, Capture arms1R—TTT TTTTTTGAATTC AAAGCGATACCCCTGAAAAGTAACT, Capture arms2F—AAAAAAAAAAGAATTCACGGGCACTGGGGAAGCTGAGTCTTA, Capture arms2R—TTTTTTTTTGGTACCCATCTGCAAGGTAGGGGGAGGGGGCGG, and cloned into pBS SK(+). The linear gap repair plasmid was transformed into EL350 cells carrying the bMQ-76E6 BAC (Liu *et al*, 2003) and gap-repaired plasmids were selected for ampicillin resistance. A *LoxP* site was inserted into intron 4 and a PGK-neomycin selection cassette flanked by *Frt* sites and a second *LoxP* site were introduced into intron 11 of the captured *Nrbp1* DNA fragment. Targeting was performed in E14J (129P2/Ola) ES cells and germline chimeras were transmitted onto a C57BL/6J background. Southern blot analysis of *Bam*HI-digested DNA was performed using 5'- and 3'-probes using standard procedures (5'-ProbeF—GAGGCTTTCTGGGTTTCCTC, 5'-ProbeR—CGGGGCACTTAGAGAAAAGA, 3'-ProbeF—GTTCGGGACTACTGGTGAGC and 3'-ProbeR—TGGCAATCAGCAATAAGACG). Mice were genotyped by PCR using the primers: A—GAA AAG GTC CGT GCA GTG TT, B—AGA TGG CAG TGC TGG AGA TT and C—CAA GCG TTC TTG TTC AGA CG. Male *Nrbp1* mice carrying the unmodified targeted allele of *Nrbp1* were crossed with either *CMV-Cre* (Su *et al*, 2002) or *129S4/SvJaeSor-Gt(ROSA)26Sor^{tm1(FLP1)Dym/J}* (*FLPeR*) mice (Farley *et al*, 2000) to produce *Nrbp1*^{+/-} and *Nrbp1*^{fllox/+} mice, respectively. *Rosa^{CreERT2/+}* mice (Vooijs *et al*, 2001) were used for somatic deletion of *Nrbp1*, and Cre-mediated site-specific recombination was performed in mice aged 7–8 weeks carrying the *Rosa^{CreERT2/+}* allele by intraperitoneal injection with either 100 µl of 40 mg/ml tamoxifen base in sunflower oil for three consecutive days or 100 µl of 10 mg/ml tamoxifen base in sunflower oil for four consecutive days. Mice that became moribund were euthanized, and tissues collected and fixed in 10% neutral buffered formalin. H&E staining was performed using standard procedures. All procedures with animals were carried out in accordance with Home Office UK guidelines.

Immunohistochemistry, ISH and immunoblotting

Immunostaining was performed on 4-µm sections using the DAKO Autostainer Plus with the rabbit VECTASTAIN ELITE ABC horseradish peroxidase kit (Vector Laboratories). For primary antibodies, see Supplementary methods. In all cases, a total of 30 crypts/villi were counted from the small intestine of four *Nrbp1*^{fllox/fllox} *Rosa^{CreERT2/+}* and control mice. Four lengths of intestinal epithelium were photographed and used to estimate crypt numbers of *Nrbp1*^{fllox/fllox} *Rosa^{CreERT2/+}*, *Nrbp1*^{fllox/fllox} *Rosa^{CreERT2/+}* and *Nrbp1*^{fllox/+} *Rosa^{CreERT2/+}* mice (four of each genotype). All comparisons were made using the Mann-Whitney *U*-test. Western blotting was performed using standard methods. For primary antibodies see Supplementary methods. Activation of Ras was analysed using Active Ras Pull-Down Detection Kit, which contains GST-Raf1-RBD fusion protein (Thermo scientific) in accordance with the

manufacturer's instructions. ISH was performed with 6- μ m sections on the automated Ventana Discovery platform with RiboMap and BlueMap Kits (Ventana) and DIG-labelled riboprobes (primers for generating probes are available in the Supplementary methods). Immunoprecipitations were performed with either HEK293 cells or mouse embryonic stem cells using a FLAG Immunoprecipitation Kit (Sigma). HEK293 cells were transiently transfected with the following expression plasmids: NRBP1-Flag-MSCV, pcDNA3-myc-CUL5 (Ohta *et al*, 1999) and c-Myc-Elongin B and HSV-Elongin C (Brower *et al*, 1999). Elongin B and Elongin C siRNAs pools were purchased from Thermo scientific. ES cells were stably integrated with NRBP1-Flag-MSCV after selection with neomycin.

qRT-PCR and microarray analysis

Total RNA was isolated from snap-frozen small intestine using TRIzol (Invitrogen), DNase treated using Turbo DNase (Ambion) and 2 μ g total RNA reverse transcribed using the BD Sprint kit with random hexamers (ABI) according to the manufacturer's protocols. qRT-PCRs were performed with SYBR Green (ABI) on the ABI StepOnePlus Real-Time PCR Systems in accordance with the manufacturer's instructions (see Supplementary methods for primer sequences). The final quantitation was determined using the standard curve method relative to the house-keeping genes *Gapdh* or *Actb*. Data were statistically analysed using ANOVA. Microarray analysis was performed on total RNA using the Illumina mouse-6 expression beadchip version 2 platform (Illumina) by standard procedures. Probe summaries were calculated in BeadStudio and quantile normalised. A linear model fit was applied and the top differentially expressed genes were tabulated for each contrast using the Benjamini and Hochberg method to correct the *P*-values. The Molecular signatures database MSigDB Version 2.5 (<http://www.broadinstitute.org/gsea/msigdb/index.jsp>) was used to compute overlaps between the top and bottom 500 most differentially expressed genes to gene sets in MSigDB (Subramanian *et al*, 2005).

Tandem affinity purification mass spectrometry analysis

The protocol used for the purification of proteins has been described previously (Pardo *et al*, 2010). Briefly, HEK293 and ES cells expressing the CBP2TEV3FLAG tag were lysed and incubated with anti-FLAG M2 Dynal beads (Sigma). TEV eluates from mouse ES cells were subsequently incubated with calmodulin resin (Stratagene), from which protein complexes were eluted by Ca chelation with EGTA. For single affinity purifications from HEK293 cells, the second purification step was omitted. EGTA and TEV eluates were separated by one-dimensional SDS electrophoresis. Gel lanes were excised, digested with trypsin and peptides extracted with 0.5% formic acid–50% acetonitrile. Peptides were analysed with on-line nanoLC-MS/MS on a LTQ FT mass spectrometer (ThermoElectron) coupled with an Ultimate

3000 Nano/Capillary HPLC System (Dionex). The LC used a PepMap C18 trap (0.3 mm id \times 5 mm, LC Packings) and a BEH C18 analytical column (75 μ m id \times 10 cm, Waters) with a 30 min linear gradient of 4–32% CH₃CN/0.1% formic acid. The LTQ FT was operated in standard data dependent acquisition. The survey scans (*m/z* 400–2000) were acquired on the FT-ICR at a resolution of 100 000 at *m/z* 400. The top four multiply charged ions were subject to MS/MS in the linear ion trap at an isolation width of 2 Th. Dynamic exclusion width was set at \pm 20 p.p.m. for 45 s. The automatic gain control target value was regulated at 5E5 for FT and 1E4 for the ion trap, with maximum injection time at 1000 ms for FT and 200 ms for ion trap, respectively. The raw files were processed with BioWorks (Thermo). Database searches were performed with Mascot v.2.2 (Matrix Science) against the Human or mouse IPI database (v. December 2008). The search parameters were: Trypsin/P with two missed cleavages, 10 p.p.m. mass tolerance for MS, 0.5-Da tolerance for MS/MS, fixed modification carbamidomethyl (C), and variable modifications of Acetyl (Protein N-term), Deamidated (NQ), Dioxidation (M), Formyl (N-term), Gln->pyro-Glu (N-term Q), Methyl (E) and Oxidation (M). Decoy database searches were performed at the same time as the real searches, resulting in false discovery rates under 5%.

Supplementary data

Supplementary data are available at *The EMBO Journal* Online (<http://www.embojournal.org>).

Acknowledgements

Work in the DJ Adams laboratory and in the MJ Arends laboratory is funded by Cancer Research UK (CR-UK) and the Wellcome Trust. Work in the AG Fraser laboratory is funded by CCS. LvdW is supported by a Kay Kendall Leukaemia Fund fellowship. GBP is funded by an MRC Career Development Award (G0600127). GP is a Pfizer Fellow of the Life Sciences Research Foundation. We thank Team 17, 77 and 83 of the Wellcome Trust Sanger Institute for their technical support and to Owen Sansom for helping us establish the organoid culture system.

Author contributions: CHW, CC, LvdW, GP, MP, TG, LY, JC, GBP, REM, DJW and NHM performed the experiments. AGR performed the computational analysis. MJA performed the histopathological analysis. MJA, AGF and DJA led the project. CHW, LvdW and DJA wrote the paper.

Conflict of interest

The authors declare that they have no conflict of interest.

References

- Adams DJ, Quail MA, Cox T, van der Weyden L, Gorick BD, Su Q, Chan WI, Davies R, Bonfield JK, Law F, Humphray S, Plumb B, Liu P, Rogers J, Bradley A (2005) A genome-wide, end-sequenced 129Sv BAC library resource for targeting vector construction. *Genomics* **86**: 753–758
- Barker N, Ridgway RA, van Es JH, van de Wetering M, Begthel H, van den Born M, Danenberg E, Clarke AR, Sansom OJ, Clevers H (2009) Crypt stem cells as the cells-of-origin of intestinal cancer. *Nature* **457**: 608–611
- Barker N, van Es JH, Kuipers J, Kujala P, van den Born M, Cozijnsen M, Haegbarth A, Korving J, Begthel H, Peters PJ, Clevers H (2007) Identification of stem cells in small intestine and colon by marker gene *Lgr5*. *Nature* **449**: 1003–1007
- Battle E, Henderson JT, Begthel H, van den Born MM, Sancho E, Huls G, Meeldijk J, Robertson J, van de Wetering M, Pawson T, Clevers H (2002) Beta-catenin and TCF mediate cell positioning in the intestinal epithelium by controlling the expression of EphB/ephrinB. *Cell* **111**: 251–263
- Beitel GJ, Clark SG, Horvitz HR (1990) *Caenorhabditis elegans* ras gene let-60 acts as a switch in the pathway of vulval induction. *Nature* **348**: 503–509
- Berset T, Hoier EF, Battu G, Canevascini S, Hajnal A (2001) Notch inhibition of RAS signaling through MAP kinase phosphatase LIP-1 during *C. elegans* vulval development. *Science* **291**: 1055–1058
- Boudeau J, Miranda-Saavedra D, Barton GJ, Alessi DR (2006) Emerging roles of pseudokinases. *Trends Cell Biol* **16**: 443–452
- Brower CS, Shilatfard A, Mather T, Kamura T, Takagi Y, Haque D, Treharne A, Foundling SI, Conaway JW, Conaway RC (1999) The elongin B ubiquitin homology domain. Identification of Elongin B sequences important for interaction with Elongin C. *J Biol Chem* **274**: 13629–13636
- Castagna M, Takai Y, Kaibuchi K, Sano K, Kikkawa U, Nishizuka Y (1982) Direct activation of calcium-activated, phospholipid-dependent protein kinase by tumor-promoting phorbol esters. *J Biol Chem* **257**: 7847–7851
- Dobens L, Jaeger A, Peterson JS, Raftery LA (2005) Bunched sets a boundary for Notch signaling to pattern anterior eggshell structures during *Drosophila* oogenesis. *Dev Biol* **287**: 425–437
- Dobens LL, Peterson JS, Treisman J, Raftery LA (2000) *Drosophila* bunched integrates opposing DPP and EGF signals to set the operculum boundary. *Development* **127**: 745–754
- Dohrmann CE, Belaousoff M, Raftery LA (1999) Dynamic expression of TSC-22 at sites of epithelial-mesenchymal interactions during mouse development. *Mech Dev* **84**: 147–151

- Duan DR, Pause A, Burgess WH, Aso T, Chen DY, Garrett KP, Conaway RC, Conaway JW, Linehan WM, Klausner RD (1995) Inhibition of transcription elongation by the VHL tumor suppressor protein. *Science* **269**: 1402–1406
- Farley FW, Soriano P, Steffen LS, Dymecki SM (2000) Widespread recombinase expression using FLP_{er} (flipper) mice. *Genesis* **28**: 106–110
- Finch AJ, Soucek L, Junttila MR, Swigart LB, Evan GI (2009) Acute overexpression of Myc in intestinal epithelium recapitulates some but not all the changes elicited by Wnt/beta-catenin pathway activation. *Mol Cell Biol* **29**: 5306–5315
- Fraser AG, Kamath RS, Zipperlen P, Martinez-Campos M, Sohrmann M, Ahringer J (2000) Functional genomic analysis of *C. elegans* chromosome I by systematic RNA interference. *Nature* **408**: 325–330
- Gluderer S, Brunner E, Germann M, Jovaisaite V, Li C, Rentsch CA, Hafen E, Stocker H (2010) Madm (Mlf1 adapter molecule) cooperates with Bunched A to promote growth in *Drosophila*. *J Biol* **9**: 9
- Hajnal A, Whitfield CW, Kim SK (1997) Inhibition of *Caenorhabditis elegans* vulval induction by gap-1 and by let-23 receptor tyrosine kinase. *Genes Dev* **11**: 2715–2728
- Hammell CM, Lubin I, Boag PR, Blackwell TK, Ambros V (2009) nhl-2 modulates microRNA activity in *Caenorhabditis elegans*. *Cell* **136**: 926–938
- Hameyer D, Loonstra A, Eshkind L, Schmitt S, Antunes C, Groen A, Bindels E, Jonkers J, Krimpenfort P, Meuwissen R, Rijswijk L, Bex A, Berns A, Bockamp E (2007) Toxicity of ligand-dependent Cre recombinases and generation of a conditional Cre deleter mouse allowing mosaic recombination in peripheral tissues. *Physiol Genomics* **31**: 32–41
- Hochedlinger K, Yamada Y, Beard C, Jaenisch R (2005) Ectopic expression of Oct-4 blocks progenitor-cell differentiation and causes dysplasia in epithelial tissues. *Cell* **121**: 465–477
- Homig-Holzel C, van Doorn R, Vogel C, Germann M, Cecchini MG, Verdegaal E, Peeper DS (2011) Antagonistic TSC22D1 variants control BRAF(E600)-induced senescence. *EMBO J* **30**: 1753–1765
- Hooper JD, Baker E, Ogbourne SM, Sutherland GR, Antalis TM (2000) Cloning of the cDNA and localization of the gene encoding human NRBP, a ubiquitously expressed, multidomain putative adapter protein. *Genomics* **66**: 113–118
- Jay P, Ji JW, Marsollier C, Taviaux S, Berge-Lefranc JL, Berta P (1996) Cloning of the human homologue of the TGF beta-stimulated clone 22 gene. *Biochem Biophys Res Commun* **222**: 821–826
- Kamath RS, Fraser AG, Dong Y, Poulin G, Durbin R, Gotta M, Kanapin A, Le Bot N, Moreno S, Sohrmann M, Welchman DP, Zipperlen P, Ahringer J (2003) Systematic functional analysis of the *Caenorhabditis elegans* genome using RNAi. *Nature* **421**: 231–237
- Kamura T, Burian D, Yan Q, Schmidt SL, Lane WS, Querido E, Branton PE, Shilatifard A, Conaway RC, Conaway JW (2001) Muf1, a novel Elongin BC-interacting leucine-rich repeat protein that can assemble with Cul5 and Rbx1 to reconstitute a ubiquitin ligase. *J Biol Chem* **276**: 29748–29753
- Kibel A, Iliopoulos O, DeCaprio JA, Kaelin Jr. WG (1995) Binding of the von Hippel-Lindau tumor suppressor protein to Elongin B and C. *Science* **269**: 1444–1446
- Koo BK, Stange DE, Sato T, Karthaus W, Farin HF, Huch M, van Es JH, Clevers H (2011) Controlled gene expression in primary Lgr5 organoid cultures. *Nat Methods* **9**: 81–83
- Liu P, Jenkins NA, Copeland NG (2003) A highly efficient recombining-based method for generating conditional knockout mutations. *Genome Res* **13**: 476–484
- Ma Y, Cui W, Yang J, Qu J, Di C, Amin HM, Lai R, Ritz J, Krause DS, Chai L (2006) SALL4, a novel oncogene, is constitutively expressed in human acute myeloid leukemia (AML) and induces AML in transgenic mice. *Blood* **108**: 2726–2735
- Madison BB, Braunstein K, Kuizon E, Portman K, Qiao XT, Gumucio DL (2005) Epithelial hedgehog signals pattern the intestinal crypt-villus axis. *Development* **132**: 279–289
- Mahroun N, Redwine WB, Florens L, Swanson SK, Martin-Brown S, Bradford WD, Staehling-Hampton K, Washburn MP, Conaway RC, Conaway JW (2008) Characterization of Cullin-box sequences that direct recruitment of Cul2-Rbx1 and Cul5-Rbx2 modules to Elongin BC-based ubiquitin ligases. *J Biol Chem* **283**: 8005–8013
- Muncan V, Sansom OJ, Tertoolen L, Phesse TJ, Begthel H, Sancho E, Cole AM, Gregorieff A, de Alboran IM, Clevers H, Clarke AR (2006) Rapid loss of intestinal crypts upon conditional deletion of the Wnt/Tcf-4 target gene *c-Myc*. *Mol Cell Biol* **26**: 8418–8426
- Nakamura H, Kishi Y, Pajares MA, Rando RR (1989) Structural basis of protein kinase C activation by tumor promoters. *Proc Natl Acad Sci USA* **86**: 9672–9676
- Ohta T, Michel JJ, Schottelius AJ, Xiong Y (1999) ROC1, a homolog of APC11, represents a family of cullin partners with an associated ubiquitin ligase activity. *Mol Cell* **3**: 535–541
- Pardo M, Lang B, Yu L, Prosser H, Bradley A, Babu MM, Choudhary J (2010) An expanded Oct4 interaction network: implications for stem cell biology, development, and disease. *Cell Stem Cell* **6**: 382–395
- Poinat P, De Arcangelis A, Sookharea S, Zhu X, Hedgecock EM, Labouesse M, Georges-Labouesse E (2002) A conserved interaction between beta1 integrin/PAT-3 and Nck-interacting kinase/MIG-15 that mediates commissural axon navigation in *C. elegans*. *Curr Biol* **12**: 622–631
- Reines D, Conaway RC, Conaway JW (1999) Mechanism and regulation of transcriptional elongation by RNA polymerase II. *Curr Opin Cell Biol* **11**: 342–346
- Rual JF, Venkatesan K, Hao T, Hirozane-Kishikawa T, Dricot A, Li N, Berriz GF, Gibbons FD, Dreze M, Ayivi-Guedehoussou N, Klitgord N, Simon C, Boxem M, Milstein S, Rosenberg J, Goldberg DS, Zhang LV, Wong SL, Franklin G, Li S *et al* (2005) Towards a proteome-scale map of the human protein-protein interaction network. *Nature* **437**: 1173–1178
- Sansom OJ, Reed KR, Hayes AJ, Ireland H, Brinkmann H, Newton IP, Battle E, Simon-Assmann P, Clevers H, Nathke IS, Clarke AR, Winton DJ (2004) Loss of Apc in vivo immediately perturbs Wnt signaling, differentiation, and migration. *Genes Dev* **18**: 1385–1390
- Sato T, Vries RG, Snippert HJ, van de Wetering M, Barker N, Stange DE, van Es JH, Abo A, Kujala P, Peters PJ, Clevers H (2009) Single Lgr5 stem cells build crypt-villus structures in vitro without a mesenchymal niche. *Nature* **459**: 262–265
- Shuai X, Zhou D, Shen T, Wu Y, Zhang J, Wang X, Li Q (2009) Overexpression of the novel oncogene SALL4 and activation of the Wnt/beta-catenin pathway in myelodysplastic syndromes. *Cancer Genet Cytogenet* **194**: 119–124
- Solari F, Ahringer J (2000) NURD-complex genes antagonise Ras-induced vulval development in *Caenorhabditis elegans*. *Curr Biol* **10**: 223–226
- Su H, Mills AA, Wang X, Bradley A (2002) A targeted X-linked CMV-Cre line. *Genesis* **32**: 187–188
- Subramanian A, Tamayo P, Mootha VK, Mukherjee S, Ebert BL, Gillette MA, Paulovich A, Pomeroy SL, Golub TR, Lander ES, Mesirov JP (2005) Gene set enrichment analysis: a knowledge-based approach for interpreting genome-wide expression profiles. *Proc Natl Acad Sci USA* **102**: 15545–15550
- Treisman JE, Lai ZC, Rubin GM (1995) Short-sighted acts in the decapentaplegic pathway in *Drosophila* eye development and has homology to a mouse TGF-beta-responsive gene. *Development* **121**: 2835–2845
- Ushiku T, Shinozaki A, Shibahara J, Iwasaki Y, Tateishi Y, Funata N, Fukayama M (2010) SALL4 represents fetal gut differentiation of gastric cancer, and is diagnostically useful in distinguishing hepatoid gastric carcinoma from hepatocellular carcinoma. *Am J Surg Pathol* **34**: 533–540
- Vooijs M, Jonkers J, Berns A (2001) A highly efficient ligand-regulated Cre recombinase mouse line shows that LoXP recombination is position dependent. *EMBO Rep* **2**: 292–297
- Voorhoeve PM, Agami R (2003) The tumor-suppressive functions of the human INK4A locus. *Cancer Cell* **4**: 311–319
- Warren M, Wang W, Spiden S, Chen-Murphy D, Tannahill D, Steel KP, Bradley A (2007) A Sall4 mutant mouse model useful for studying the role of Sall4 in early embryonic development and organogenesis. *Genesis* **45**: 51–58



The EMBO Journal is published by Nature Publishing Group on behalf of European Molecular Biology Organization. This article is licensed under a Creative Commons Attribution-NonCommercial-Share Alike 3.0 Licence. [<http://creativecommons.org/licenses/by-nc-sa/3.0/>]